On the Structure of Transient Upwelling Events[1]

G. T. CSANADY

Woods Hole Oceanographic Institution, Woods Hole, MA 02543

(Manuscript received 27 May 1981, in final form 26 October 1981)

ABSTRACT

Nearshore transects, following the development of transient coastal upwelling, characteristically show "intermediate" density fluid occupying the immediate nearshore band. Large cross-shore particle excursions during the development of upwelling may be inferred from before and after transects, and the movement of surface layers seaward, intermediate density fluid shoreward through a distance of the order of kilometers, and the bottom layers also shoreward by a lesser amount. Some inevitable vertical mixing together with the large cross-shore displacements results in efficient cross-shore mass exchange.

The main dynamical features of similar events may be investigated by means of three-layer models. Linear theory is conveniently discussed first, the conclusions of which are easily generalized to multilayer models. Finite-amplitude (i.e., "full") upwelling is then considered using a potential-vorticity conserving impulsive model. The results show that the wind "peels" off the surface layer over which the wind stress is effectively distributed. Thus the next lightest layer becomes exposed to the atmosphere. The lower layers generally respond in the barotropic mode, becoming "equally stretched" on the removal of the surface layer, except within a distance of the order of the baroclinic radius of deformation from the pycnocline outcropping. The maximum velocity of the jet associated with the pycnocline outcropping is limited to an effective densimetric velocity. Cross-shore displacements behave similarly in the model and the observed cases.

1. Introduction

A strong impulse of longshore wind, directed so that the coast is to the left looking downwind in the Northern Hemisphere, if acting over stratified coastal waters is well known to cause a drop of water temperature at the coast, due to the "upwelling" of water from deeper layers. Transient events of this kind along the Oregon coast (Halpern, 1976; Huyer *et al.*, 1979) or in the Great Lakes (Mortimer, 1963; Csanady, 1977) have been well documented. A realistic idealization is to think of two layers of fluid of slightly different density, the top layer being subject to sudden longshore acceleration. In the course of adjustment to geostrophic equilibrium the interface moves upward, but only within a relatively short distance from the coast (scaled by the internal radius of deformation), and if the wind impulse is strong enough, comes to intersect the free surface and even move some distance offshore. A two-layer inertial adjustment model, neglecting interface and bottom friction, quite satisfactorily accounts for many observed characteristics of transient upwelling events, including in particular the distance offshore where the density interface is found after adjustment to geostrophic equilibrium (Csanady, 1977).

In the two-layer model, bottom layer fluid comes to occupy the nearshore band following adjustment. The observations, however, rarely show coastal water temperatures quite as low as are found in deep water. In the Great Lakes, for example, water temperatures below ~30 m are usually 5°C or lower in early and mid summer. Coastal temperatures after the development of upwelling are, on the other hand, typically 10°C. While the effects of vertical mixing and of longshore advection are sometimes difficult to separate from those of inertial adjustment, a perusal of the records of observations on upwelling events leaves one with the distinct impression that the inertial adjustment alone (if it could be observed in isolation from vertical mixing and longshore advection) would already leave fluid of intermediate density, not bottom water, in the coastal band.

Consider, for example, an upwelling event observed along the north shore of Lake Ontario during the International Field Year on the Great Lakes (IFYGL). Figs. 1 and 2 show before and after isotherms in a coastal transect off Oshawa, Ontario, bracketing an eastward wind stress impulse (I) estimated to have been 9 $m^2 s^{-1}$ (Csanady, 1973). This followed an earlier, *westward* impulse of $I = 2.5$ $m^2 s^{-1}$, which was the cause of the downwarping of the isotherms visible in Fig. 1. Starting from horizontal isotherms the algebraic total may be taken to have been $I = 6.5$ $m^2 s^{-1}$, eastward. Using the formula in Csanady (1977), and a two layer idealization of the temperature structure with top-layer depth $h_t = 7$

[1] Woods Hole Oceanographic Institution Contribution No. 4893.

0022-3670/82/010084-13$07.25

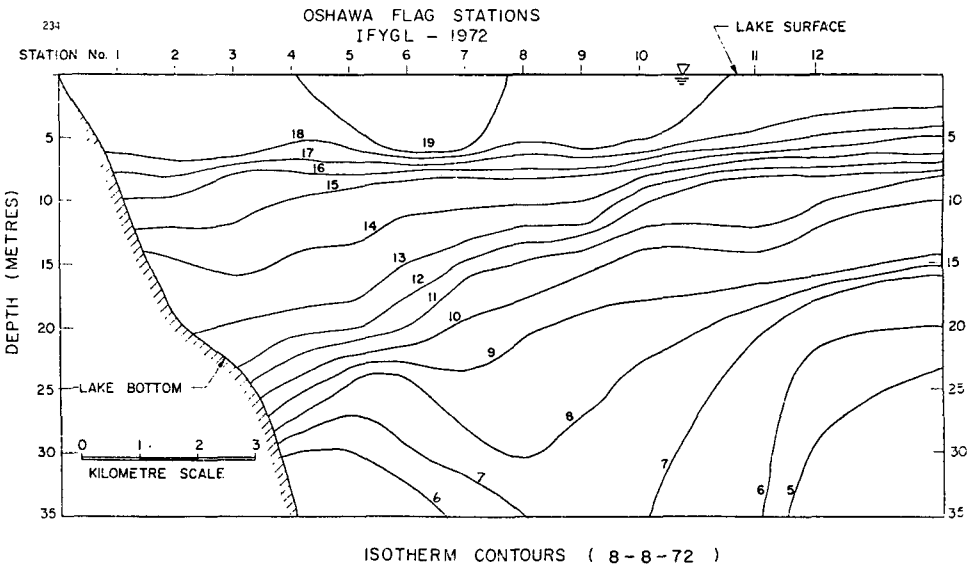

FIG. 1. Temperature distribution in transect across coastal waters of Lake Ontario off Oshawa, Ontario, prior to an eastward wind impulse in early August, with a shallow thermocline.

m, the expected offshore displacement of the thermocline outcropping is estimated at 6 km or so. Insofar as one may regard the 16°C isotherm as the thermocline, the result is accurate.

It is also clear, however, that a two-layer view of the event is incomplete and in some respects misleading. Nearshore surface temperatures remained around 13°C, and the 12°C isotherm, which formed the center of the thermocline after the upwelling event, came no closer to the surface than ~5 m, except at station 1, 1 km from the shore. The tongue of bottom water reaching shoreward at the innermost stations is legitimately regarded as a bottom Ekman layer intrusion associated with the strong eastward flow observed at these stations at all levels. As far as one can judge, inertial effects brought the 12°C isotherm to 5 m from an equilibrium depth of perhaps 10 m, in an upwelling event in which the surface mixed-layer moved some 6 km offshore.

A somewhat similar, perhaps even more striking event is shown in Figs. 3 and 4, observed in September 1971 in the same location. The thermocline on this occasion was sharp and much deeper. The eastward wind impulse between the two illustrations was

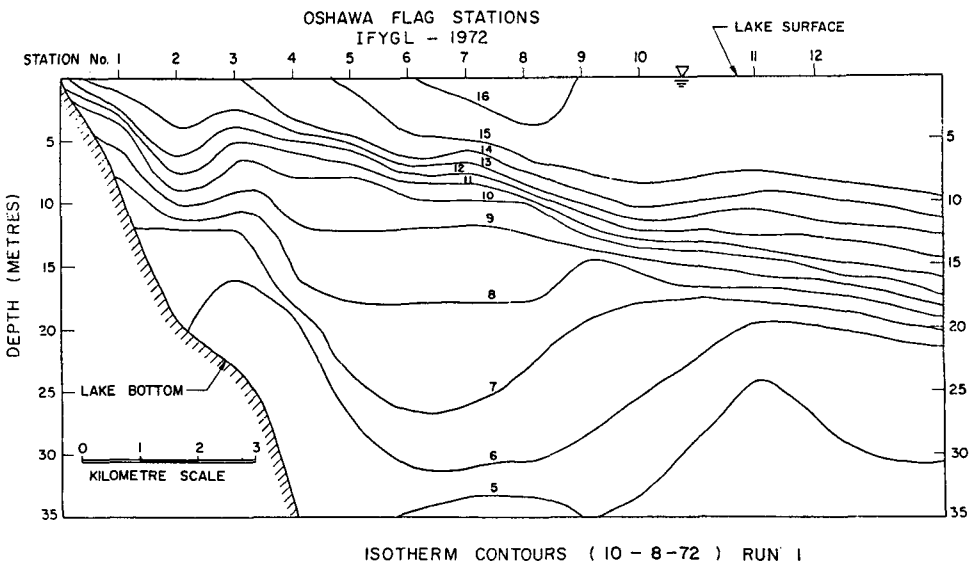

FIG. 2. As Fig. 1 except following eastward wind impulse.

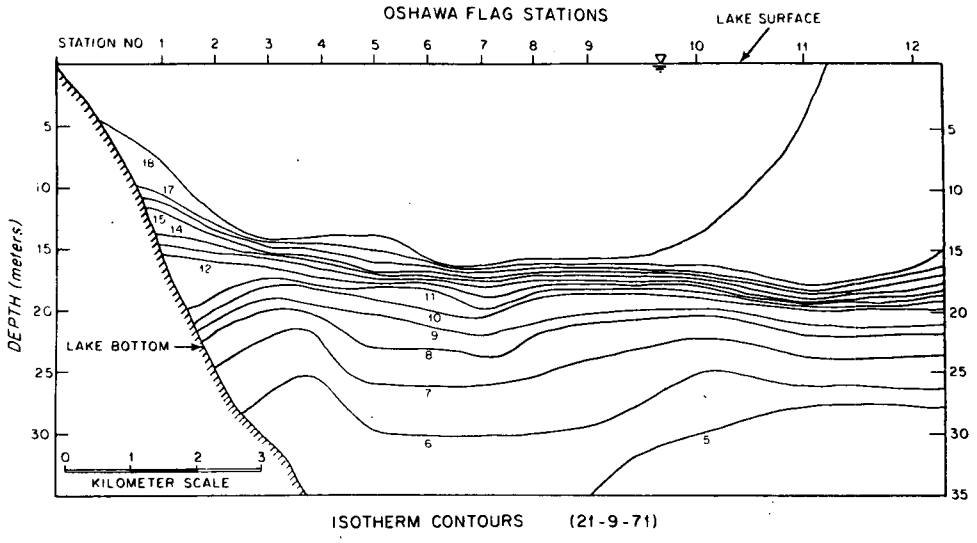

FIG. 3. As Fig. 1 except in late September, prior to eastward wind impulse, with deep thermocline.

about 5 $m^2 s^{-1}$. Its effect was to "peel off" isotherms above about 15°C, but raise the main thermocline after the upwelling (12°C isotherms) only to ~5 m from the surface.

The structure of upwelling events in *small* lakes, due in that case to offshore wind, with earth rotation effects being negligible, has been discussed in a pioneering paper by Mortimer (1952). Fig. 5, reproduced from Mortimer's paper, shows schematically the behavior of a three-layer laboratory model under increasingly violent winds. Mortimer points out that case (a) of his figure is reminiscent of observations in lakes in which "steady winds produce a very sharp thermocline at the leeward end, in contrast to a spreading out of the isotherms at the windward end of the basin." Horizontal fluid particle displacements which can be inferred from these illustrations are large in the top and intermediate layers, and relatively small in the bottom layer. Large horizontal relative excursions of fluid in the three layers thus characterize the response to wind.

From the earlier illustrations it is clear that similar large cross-shore excursions occur in large basins within a few kilometers from the shore. These possess considerable dynamical importance, because the Coriolis force, associated with a 1 km cross-shore displacement, if unresisted, generates a longshore velocity of 0.1 m s^{-1}. In this manner, layers not directly acted on by the wind acquire longshore velocity. The layer that is directly influenced by the wind,

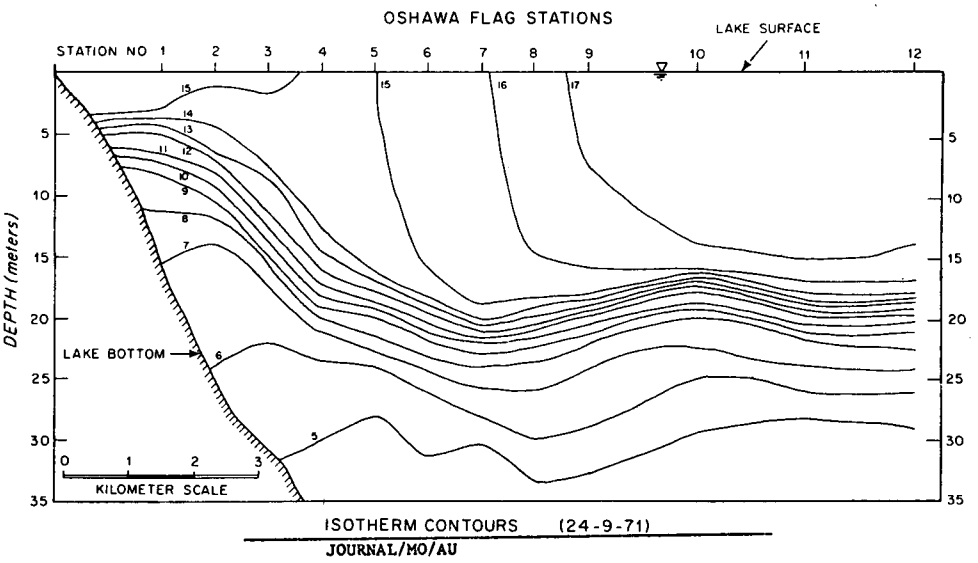

FIG. 4. As Fig. 3 except following eastward wind impulse.

on the other hand, deflects to the right, which is the reason why a longshore wind leaving the coast to the left becomes the main cause of upwelling. Without further investigation it is not clear, however, whether the analogy between cross-shore wind effects in a small lake, and longshore wind effects in a large basin, extends to the behavior of intermediate and bottom layers. Are there likely to be effects similar to those shown in Fig. 5 in large basins? Are the isopycnals in the thermocline likely to open up on an upwelling shore, to condense on a downwelling shore? Figs. 1–4 suggest some degree of correspondence, worth a theoretical investigation.

As pointed out before, vertical mixing under strong winds, especially at night in September, cannot be neglected, nor is it clear to what extent any longshore advection complicates similar events. Nevertheless, a first step toward understanding the detailed structure of transient upwelling events in large basins may be taken by asking how an inertial model more realistic than a two-layer one would respond to sudden longshore wind, ignoring mixing and internal friction below the surface mixed layer. This question is addressed in this paper.

The analysis begins with a linearized three-layer model. The results are easily generalized in principle to a multilayer model, although they are only realistic for a small wind impulse, and small vertical displacements of the isopycnals. A standard decomposition into a set of normal modes (in the vertical) is adopted. The resulting behavior of each mode is readily seen to be the same as found by Crépon (1967) in his linear analysis of impulsively generated motions in a homogeneous fluid along a long, straight coast. The reason for including these linear theory calculations here is to exhibit the initial behavior in impulsively generated upwelling. It transpires that without a summation of all normal mode responses (i.e., without inverting the transformation to normal modes) the important physical properties of the resultant response are not revealed. In other linear theory analyses, the behavior of each excited mode is usually considered separately, as an essentially independent physical phenomenon. When the response consists of wavelike motions at incommensurable frequencies this is a plausible point of view. However, the impulsive motions discussed below depend linearly on time in each normal mode and are not reasonably regarded as independent phenomena. The matrix method of analysis adopted below leads to easy inversion of the transformation into normal modes.

Following the linear theory analysis of initial behavior, a different approach is adopted for calculating "full" upwelling, much as in Csanady (1977). The key idealization in this part of the paper is that the entire wind-stress force has been exerted impulsively, in a short enough time so that layer depths

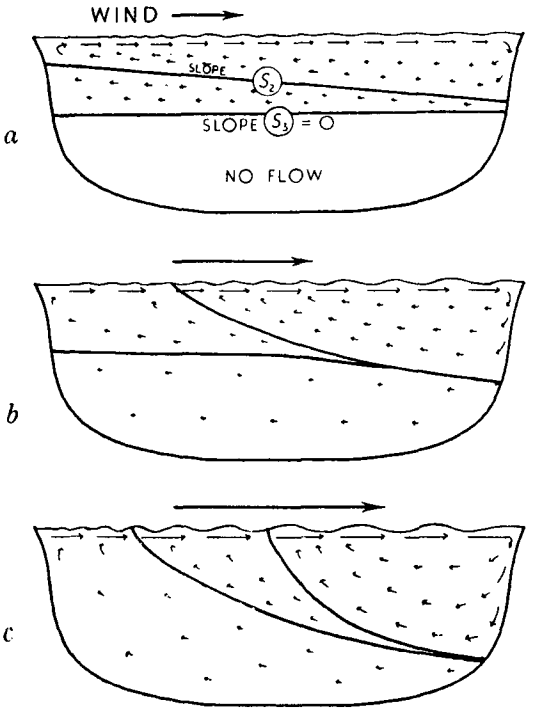

FIG. 5. Behavior of three-layer laboratory basin under winds of varying intensity; (a) gentle wind, only top interface moves appreciably; (b) moderate wind, both interfaces move; (c) strong wind, intermediate density fluid forms wedge (from Mortimer, 1952).

do not change appreciably while the wind is acting. The calculations made concern the state of geostrophic equilibrium reached *following* the action of the wind, so that only the impulse (time-integral) of the wind stress appears in the results. Clearly, there is some over-idealization in this approach, because the wind lasts in practice long enough for the surface-layer depth to change appreciably near shore due to offshore transport. The dynamical importance of this is highlighted by the potential vorticity tendency equation for a layer of depth h

$$\frac{d}{dt}\left(\frac{\omega + f}{h}\right) = \frac{1}{h}\,\mathrm{curl}\left(\frac{\tau}{\rho h}\right),$$

where ω is vorticity, f the Coriolis parameter and τ/ρ kinematic wind stress. In the theory developed for finite amplitude upwelling, the right-hand side of this equation, integrated over the period of wind action, is regarded as vanishingly small, so that the potential vorticity of each water column is the same after the development of full upwelling as before the application of the wind.

Calculations made for a two-layer model, with a crude allowance for potential vorticity changes in the course of wind action, show (Csanady, 1977) that the response is modified in some respects by the fact

that the top layer becomes shallower as the upwelling develops, i.e., the shape of the interface becomes different from that which is calculated with constant potential vorticity. However, the gross behavior remains the same. Perhaps it is not necessary to stress this point further: the idealized calculations should provide some useful physical insight, but they clearly have their limitations.

From a physical point of view, the main justification for an impulsive force model of wind action is that most of the drag force during a storm is exerted on the water in a matter of 5–10 h, while the longshore currents generated, and the associated upwelled thermocline structure, persist for days. The model of impulsive force application, followed by adjustment to geostrophic equilibrium with no wind stress acting, is certainly more realistic than the assumption of a constant wind would be. This is the case, at least in midlatitudes, and such a model should apply with some degree of realism to upwelling in the Great Lakes or along the Oregon Coast.

2. Three-layer fluid, small displacements

Consider three layers of fluid of equilibrium depths h_1, h_2, h_3, densities ρ_1, ρ_2, ρ_3, the total depth $H = h_1 + h_2 + h_3$ being constant (Fig. 6). Let the surface and the interfaces be displaced vertically by the distances ζ_1, ζ_2 and ζ_3, all small compared to the smallest of h_i. Supposing the pressure to be hydrostatic, the linearized equations of motion on a rotating earth take the form

$$\left.\begin{aligned}
&\frac{\partial u_1}{\partial t} - fv_1 = -g\frac{\partial \zeta_1}{\partial x} + \frac{F_x}{h_1}\\
&\frac{\partial v_1}{\partial t} + fu_1 = -g\frac{\partial \zeta_1}{\partial y} + \frac{F_y}{h_1}\\
&\frac{\partial u_2}{\partial t} - fv_2 = -g\frac{\rho_1}{\rho_2}\frac{\partial \zeta_1}{\partial x} - g\left(1 - \frac{\rho_1}{\rho_2}\right)\frac{\partial \zeta_2}{\partial x}\\
&\frac{\partial v_2}{\partial t} + fu_2 = -g\frac{\rho_1}{\rho_2}\frac{\partial \zeta_1}{\partial y} - g\left(1 - \frac{\rho_1}{\rho_2}\right)\frac{\partial \zeta_2}{\partial y}\\
&\frac{\partial u_3}{\partial t} - fv_3 = -g\frac{\rho_1}{\rho_3}\frac{\partial \zeta_1}{\partial x} - g\frac{\rho_2}{\rho_3}\left(1 - \frac{\rho_1}{\rho_2}\right)\frac{\partial \zeta_2}{\partial x}\\
&\qquad\qquad - g\left(1 - \frac{\rho_2}{\rho_3}\right)\frac{\partial \zeta_3}{\partial x}\\
&\frac{\partial v_3}{\partial t} + fu_3 = -g\frac{\rho_1}{\rho_3}\frac{\partial \zeta_1}{\partial y} - g\frac{\rho_2}{\rho_3}\left(1 - \frac{\rho_1}{\rho_2}\right)\frac{\partial \zeta_2}{\partial y}\\
&\qquad\qquad - g\left(1 - \frac{\rho_2}{\rho_3}\right)\frac{\partial \zeta_3}{\partial y}
\end{aligned}\right\}, \quad (1)$$

where f is the Coriolis parameter, F_x, F_y are kinematic wind stress components, u_i and v_i ($i = 1, 2, 3$) are x and y components of the velocity in the three layers and g is acceleration of gravity. The three equations of continuity are

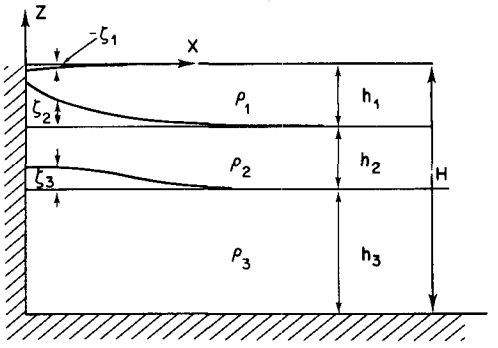

FIG. 6. Three layers of fluid along straight, infinite coast, responding to longshore wind toward positive y (into drawing).

$$\left.\begin{aligned}
&\frac{\partial u_1}{\partial x} + \frac{\partial v_1}{\partial y} = -\frac{1}{h_1}\frac{\partial}{\partial t}(\zeta_1 - \zeta_2)\\
&\frac{\partial u_2}{\partial x} + \frac{\partial v_2}{\partial y} = -\frac{1}{h_2}\frac{\partial}{\partial t}(\zeta_2 - \zeta_3)\\
&\frac{\partial u_3}{\partial x} + \frac{\partial v_3}{\partial y} = -\frac{1}{h_2}\frac{\partial \zeta_3}{\partial t}
\end{aligned}\right\}. \quad (2)$$

Let a linear combination of the equations of motion (1) be formed by multiplying the equations of the first layer by a constant a, the second by b, the third by c and adding. On the right-hand side of this combination one finds x and y gradients of the pressure variable:

$$\Pi^* = \left(a + b\frac{\rho_1}{\rho_2} + c\frac{\rho_1}{\rho_3}\right)\zeta_1 + \left(b - b\frac{\rho_1}{\rho_2} + c\frac{\rho_2}{\rho_3} - c\frac{\rho_1}{\rho_3}\right)\zeta_2 + \left(c - c\frac{\rho_2}{\rho_3}\right)\zeta_3. \quad (3)$$

A similar combination of the equations of continuity has on its right-hand side the time derivative of

$$\Pi = \frac{a}{h_1}\zeta_1 + \left(\frac{b}{h_2} - \frac{a}{h_1}\right)\zeta_2 + \left(\frac{c}{h_3} - \frac{b}{h_2}\right)\zeta_3. \quad (4)$$

Let the constants a, b, c be chosen so that Π and Π^* are the same, except for a constant multiplier β:

$$\Pi^* \equiv \beta\Pi, \quad (5)$$

where the identity is to hold for whatever values of ζ_1, ζ_2 and ζ_3. Equating the coefficients of ζ_1, ζ_2 and ζ_3 in this identity, one finds three equations for a, b and c. After some minor manipulations one can express these equations in the following form, in matrix notation:

$$\begin{bmatrix} 1-\frac{\beta}{h_1} & \frac{\rho_1}{\rho_2} & \frac{\rho_1}{\rho_3} \\ 1 & 1-\frac{\beta}{h_2} & \frac{\rho_2}{\rho_3} \\ 1 & 1 & 1-\frac{\beta}{h_3} \end{bmatrix} \times \begin{bmatrix} a \\ b \\ c \end{bmatrix} = 0 \quad (6)$$

In order for non-trivial solutions to exist, the determinant of the square matrix must vanish. This yields a cubic equation for the multiplier β:

$$\beta^3 - H\beta^2 + \gamma H^2\beta - \alpha H^3 = 0, \quad (7)$$

where

$$\gamma = \frac{1}{H^2}(\epsilon_{12}h_1h_2 + \epsilon_{23}h_2h_3 + \epsilon_{13}h_1h_3),$$

$$\alpha = \frac{1}{H^3}\epsilon_{12}\epsilon_{23}h_1h_2h_3,$$

$$\epsilon_{12} = 1 - \frac{\rho_1}{\rho_2},$$

$$\epsilon_{23} = 1 - \frac{\rho_2}{\rho_3},$$

$$\epsilon_{13} = 1 - \frac{\rho_1}{\rho_3}.$$

In cases of practical interest, all ϵ_{ij} are small, say, of order $\epsilon = 10^{-3}$. An inspection of Eq. (7) reveals that one of the three roots β_i ($i = 1, 2, 3$) is of order H, the other two of order ϵH. The order H root is approximately

$$\beta_1 = H + O(\epsilon H). \quad (8)$$

The other two roots, $i = 2, 3$, approximately satisfy Eq. (7) with the cubic term deleted, i.e.,

$$\beta_{2,3} = \frac{H}{2}[\gamma \pm (\gamma^2 - 4\alpha)^{1/2}] + O(\epsilon^2 H). \quad (9)$$

Taking now β in Eq. (5) to be one of the three roots of Eq. (7), one of the multipliers a, b, c may be chosen arbitrarily, the other two are determined by Eqs. (6). One thus arrives at the square matrix of coefficients $[a_i, b_i, c_i]$, $i = 1, 2, 3$, the index i connecting to the root β_i. A convenient choice proves to be $c_i = h_3$ for all i, which results in

$$\left.\begin{aligned} a_i &= -h_2 - h_3 + \epsilon_{23}\frac{h_2h_3}{\beta_i} + \beta_i \\ b_i &= h_2 - \frac{\epsilon_{23}h_2h_3}{\beta_i} \\ c_i &= h_3 \end{aligned}\right\}. \quad (10)$$

Some further results are written down most concisely by changing the notation of the matrix $[a_i, b_i, c_i]$ into $[\mathbf{a}_{ij}]$, i.e., replacing a by $j = 1$, b by $j = 2$, c by $j = 3$. The multiplication of Eqs. (1) and (2) by $\mathbf{a}_{ij}$, $j = 1, 2, 3$, followed by their addition is then tantamount to the following transformation of the velocity variables:

$$\left.\begin{aligned} U_i &= \mathbf{a}_{ij}u_j \\ V_i &= \mathbf{a}_{ij}v_j \end{aligned}\right\}, \quad (11)$$

where the summation convention applies. The transformation of the pressure variables is a little more complicated, given by Eq. (4) above. On writing

$$b_{i1} = \frac{a_i}{h_1}, \quad b_{i2} = \frac{b_i}{h_2} - \frac{a_i}{h_1}, \quad b_{i3} = \frac{c_i}{h_3} - \frac{b_i}{h_2}, \quad (12)$$

the pressure transformation is expressed as

$$\Pi_i = \mathbf{b}_{ij}\zeta_j. \quad (13)$$

The forcing terms transform as

$$F_{xi} = \frac{a_i}{h_1}F_x, \quad F_{yi} = \frac{a_i}{h_1}F_y. \quad (14)$$

The transformed equations of motion and continuity now become

$$\left.\begin{aligned} &\frac{\partial U_i}{\partial t} - fV_i = -g\beta_i\frac{\partial \Pi_i}{\partial x} + F_{xi}, \quad \text{(no sums)} \\ &\frac{\partial V_i}{\partial t} + fU_i = -g\beta_i\frac{\partial \Pi_i}{\partial y} + F_{yi} \\ &\frac{\partial U_i}{\partial x} + \frac{\partial V_i}{\partial y} = -\frac{\partial \Pi_i}{\partial t} \end{aligned}\right\}, \quad (15)$$

for $i = 1, 2, 3$. The three sets of three equations of motion and continuity for each layer have thus been replaced by three sets of normal mode equations, which, unlike the original equations, are uncoupled, so that each set can be solved independently of the other two. The solution of the original equations is then found, in principle, by inverting the transformation of the variables, i.e.,

$$\left.\begin{aligned} u_j &= \frac{A_{ij}}{\Delta_a}U_i \\ v_j &= \frac{A_{ij}}{\Delta_a}V_i \\ \zeta_j &= \frac{B_{ij}}{\Delta_b}\Pi_i \end{aligned}\right\}, \quad (16)$$

where A_{ij} and B_{ij} are the cofactors of $\mathbf{a}_{ij}$ and $\mathbf{b}_{ij}$ respectively and Δ_a, Δ_b are the determinants $|\mathbf{a}_{ij}|$ and $|\mathbf{b}_{ij}|$. The three terms on the right of (16) (on expanding sums over index i) may be thought of as contributions to velocities and elevations by individual normal modes, which are simply summed.

3. Quasi-geostrophic response to sudden longshore wind

Let a longshore wind stress $F_y = F$, $F_x = 0$ be suddenly applied at $t = 0$ to the three-layer system illustrated in Fig. 6. On transformation to normal modes, each of the three sets of Eqs. (15) is to be solved in this case with $F_{xi} = 0$, $F_{yi} = a_i F/h_1$ at $t \geqslant 0$. The solution is known from homogeneous fluid theory, having been discussed in detail by Crépon (1967): it consists of a quasi-geostrophic part and near-inertial oscillations propagating from the coast into the interior with velocity $(g\beta_i)^{1/2}$. The quasi-geostrophic part is Charney's (1955) well-known coastal jet

$$\left.\begin{aligned} U_i &= \frac{a_i F}{f h_1}\left(1 - e^{-x/R_i}\right) \\ V_i &= \frac{a_i F t}{h_1} e^{-x/R_i}, \quad \text{(no sums)} \\ \Pi_i &= -\frac{a_i F t}{f R_i h_1} e^{-x/R_i} \end{aligned}\right\}, \tag{17}$$

where $R_i = f^{-1}(g\beta_i)^{1/2}$ are the three radii of deformation. The solution satisfies the boundary condition at the coast, $U_i = 0$, and reduces at infinity to Ekman transport, $U_i = a_i F/f h_1$, $V_i = 0$, $\Pi_i = 0$.

Velocities in each of the three layers are found on inverting the transformation to normal modes according to Eq. (16). Simple results are obtained for some limiting cases. Consider first cross-shore velocities at $x \gg R_i$, for any i:

$$u_j = \frac{A_{ij}}{\Delta_a} U_i = \frac{A_{ij} a_i}{\Delta_a} \cdot \frac{F}{f h_1}, \quad (x \gg R_i). \tag{18}$$

By a well-known theorem of algebra, the product sum $a_i A_{ij}$ is equal to Δ_a for $j = 1$, to zero for $j = 2$ or 3, because a_i is the first column of the matrix of which A_{ij} are the cofactors. Thus

$$u_1 = \frac{F}{f h_1}, \quad u_2 = u_3 = 0, \quad (x \gg R_i). \tag{18a}$$

The discrepancy between the first root of Eq. (7), $\beta_1 \approx H$, and the other two roots has the consequence that $R_1 \gg R_2, R_3$. "Intermediate" distances may thus be defined by

$$R_2, R_3 \ll x \ll R_1, \tag{19}$$

At such intermediate distances $U_1 \approx 0$, but $U_2 = a_2 F/f h_1$, $U_3 = a_3 F/f h_1$, according to Eq. (17). To interpret this result physically the $[a_{ij}]$ matrix needs to be examined. Neglecting terms of order ϵ from Eq. (10) this matrix is

$$[a_{ij}] \equiv \begin{bmatrix} h_1 & h_2 & h_3 \\ -h_2 + \lambda_2 h_2 - h_3 & h_2 - \lambda_2 h_2 & h_3 \\ -h_2 + \lambda_3 h_2 - h_3 & h_2 - \lambda_3 h_2 & h_3 \end{bmatrix}, \tag{20}$$

where $\lambda_2 = \epsilon_{23} h_3/\beta_2$, $\lambda_3 = \epsilon_{23} h_3/\beta_3$. Using the theorem just quoted, $a_i A_{ij} = 0$ for $j = 2$ or 3, one finds at once

$$u_2 = \frac{a_1 F}{f h_1} \frac{A_{12}}{\Delta_a} = -\frac{F}{fH} \quad (R_2, R_3 \ll x \ll R_1). \tag{21}$$

and $u_3 = u_2$, $u_1 = F/f h_1 - F/fH$. This is cross-shore Ekman drift in the top layer, and a compensating adjustment drift F/fH evenly distributed over the water column, as in a homogeneous fluid close to a coast under similar forcing. Very close to the coast $x \ll R_3$, and all cross-shore velocities vanish, $u_1 = u_2 = u_3 = 0$.

The distribution of longshore velocities v_j may similarly be inferred from (17) and (20) noting that $V_i = a_i F t/h_1$ at $x \ll R_3$, $V_i = 0$ at $x \to \infty$, and $V_1 = Ft$, $V_2 = V_3 = 0$ at "intermediate" distances defined by Eq. (19). Correspondingly,

$$\left.\begin{aligned} v_1 &= \frac{Ft}{h_1}, \; v_2 = v_3 = 0, && (x = 0) \\ v_1 = v_2 = v_3 &= \frac{Ft}{H}, && (R_2, R_3 \ll x \ll R_1) \\ v_1 = v_2 = v_3 &= 0, && (x \gg R_1) \end{aligned}\right\}. \tag{22}$$

These asymptotic results are very much as one finds from a two-layer model, treating the bottom two layers as one, i.e., ignoring the structure of the thermocline. More interesting results emerge on calculating the interface displacements ζ_2 and ζ_3. These depend on the matrix $[b_{ij}]$, given to zeroth order in ϵ by:

$$[b_{ij}] = \begin{bmatrix} 1 & 0 & 0 \\ -\dfrac{h_2 + h_3}{h_1} + \lambda_2 \dfrac{h_2}{h_1} & \dfrac{H}{h_1} - \lambda_2 \dfrac{h_1 + h_2}{h_1} & \lambda_2 \\ \dfrac{h_2 + h_3}{h_1} + \lambda_3 \dfrac{h_2}{h_1} & \dfrac{H}{h_1} - \lambda_3 \dfrac{h_1 + h_2}{h_1} & \lambda_3 \end{bmatrix}. \tag{23}$$

As may be seen from Eq. (17), the excitation of the individual normal mode pressure variables Π_i is proportional to R_i^{-1}, hence it is much less intense for $i = 1$ than for $i = 2$, 3. Correspondingly, interface displacements are given to an adequate accuracy by

$$\left.\begin{aligned} \zeta_2 &\approx -\frac{Ft}{f h_1 \Delta_b}\left[\frac{a_2 B_{22}}{R_2} e^{-x/R_2} + \frac{a_3 B_{32}}{R_3} e^{-x/R_3}\right] \\ \zeta_3 &\approx -\frac{Ft}{f h_1 \Delta_b}\left[\frac{a_2 B_{23}}{R_2} e^{-x/R_2} + \frac{a_3 B_{33}}{R_2} e^{-x/R_3}\right] \end{aligned}\right\}. \tag{24}$$

The cofactors B_{ij} of the matrix $[b_{ij}]$ in Eq. (23) are easily calculated and, together with a_2, a_3 from Eq. (20), determine interface shapes to zeroth order.

The theoretical results are best appreciated by means of a numerical example discussed in the next section. One general result worthy of note is that, since $v_2 = v_3 = 0$ at $x = 0$, the interface shape must here have a horizontal tangent by Eqs. (1):

$$\frac{\partial \zeta_3}{\partial x} = 0, \quad (x = 0). \tag{25}$$

By contrast, $\partial \zeta_2/\partial x$ at $x = 0$ is certainly not zero, because v_1 and v_2 differ on account of the acceleration of the top layer by the wind.

4. A typical example

A typical summer situation in the coastal ocean may be modeled by the following:

$h_1 = 15$ m, $h_2 = 15$ m, $h_3 = 45$ m, $H = 75$ m; $\epsilon_{12} = 10^{-3}$, $\epsilon_{23} = 10^{-3}$; $f = 10^{-4}$ s^{-1}, $g = 10$ m s^{-2}.

It is easy to calculate

$$\lambda_2 = \frac{\epsilon_{23} h_3}{\beta_2} = 1.83772,$$

$$\lambda_3 = \frac{\epsilon_{23} h_3}{\beta_3} = 8.16228,$$

$R_1 = 274$ km, $R_2 = 4.95$ km, $R_3 = 2.35$ km.

For an impulse $Ft = 1$ m^2 s^{-1}, the interface elevations are thus calculated to be (in m)

$$\left.\begin{aligned} \zeta_2 &= 1.13e^{-x/R_2} + 1.03e^{-x/R_3} \\ \zeta_3 &= 1.56e^{-x/R_2} - 0.74e^{-x/R_3} \end{aligned}\right\}. \tag{26}$$

At the coast, where $x = 0$, these add up to 2.16 m for ζ_2 and 0.82 m for ζ_3. On integrating from the coast to infinity, one finds an excess volume of 0.8 Ft/f accommodated below the top interface and 0.6 Ft/f below the second, in accordance with the cross-shore transports calculated at intermediate distances. Closer to shore, however, there is a rearrangement of fluid: the second layer is thicker than its equilibrium depth to a distance or order R_3; beyond that it is thinner to a distance of order R_2. Fig. 7 illustrates the calculated interface shapes. The variations of the thickness of the various layers imply considerable relative motion in the cross-shore direction.

An impulse $I = Ft$ of 1 m^2 s^{-1} is quite moderate, evoked by a 7 m s^{-1} wind acting for only 3 h. An order of magnitude larger impulse is commonplace. Linear theory is clearly not valid for such cases, because the predicted interface displacement exceeds top layer thickness.

5. Finite vertical displacements

Consider therefore the practically important case where the top interface comes to intersect the free surface at some arbitrary distance $x = a$ from the coast (Fig. 8). Subject to later verification it will be supposed that the second (lower) interface does not come to the surface. The so represented "full" upwelling is taken to be produced by a sufficiently strong alongshore wind impulse toward positive y, all exerted before fluid column depths change significantly. Following this the fluid layers adjust to equilibrium. Friction is neglected (except for supposing the top layer to have been accelerated by the wind) so that the adjustment process is governed by conservation of potential vorticity. Geostrophic balance following adjustment and the equality of potential vorticity before and after, for each layer separately, yields the following set of six equations, valid at $x > a$, where three layers of fluid are present after adjustment:

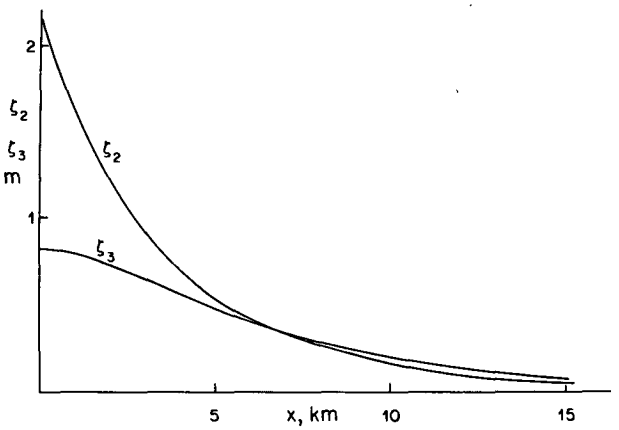

FIG. 7. Vertical displacements of top (ζ_2) and bottom (ζ_3) interfaces at different distances from the coast, calculated from linear (small perturbation) theory, for very light longshore wind impulse ($Ft = 1$ m^2 s^{-1}). For wind toward positive y, displacements are upward, for opposite wind downward.

$$\left.\begin{aligned} -fv_1 &= -g\frac{d\zeta_1}{dx} \\ -fv_2 &= -g\frac{\rho_1}{\rho_2}\frac{d\zeta_1}{dx} - g\epsilon_{12}\frac{d\zeta_2}{dx} \\ -fv_3 &= -g\frac{\rho_1}{\rho_3}\frac{d\zeta_1}{dx} - g\frac{\rho_2}{\rho_3}\epsilon_{12}\frac{d\zeta_2}{dx} - g\epsilon_{23}\frac{d\zeta_3}{dx} \\ \frac{dv_1}{dx} &= f\left(\frac{\zeta_1}{h_1} - \frac{\zeta_2}{h_1}\right) \\ \frac{dv_2}{dx} &= f\left(\frac{\zeta_2}{h_2} - \frac{\zeta_3}{h_2}\right) \\ \frac{dv_3}{dx} &= f\frac{\zeta_3}{h_3} \end{aligned}\right\}. \tag{27}$$

Eliminating the velocities between these equations, writing

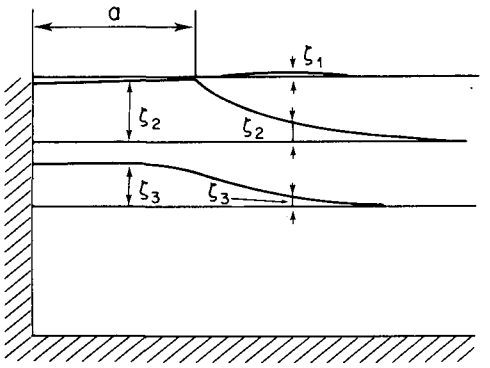

FIG. 8. Definition sketch for three-layer fluid subject to "full" upwelling, in which top density interface intersects surface.

$$\frac{d^2}{dx^2} = \frac{1}{R^2} = \frac{f^2}{g\beta} \tag{28}$$

and multiplying by β/f, the following equations for surface and interface displacements result:

$$\begin{bmatrix} 1 - \dfrac{\beta}{h_1} & \dfrac{\beta}{h_1} & 0 \\ \dfrac{\rho_1}{\rho_2} & \epsilon_{12} - \dfrac{\beta}{h_2} & \dfrac{\beta}{h_2} \\ \dfrac{\rho_1}{\rho_3} & \dfrac{\rho_2}{\rho_3} - \dfrac{\rho_1}{\rho_3} & \epsilon_{23} - \dfrac{\beta}{h_3} \end{bmatrix} \times \begin{bmatrix} \zeta_1 \\ \zeta_2 \\ \zeta_3 \end{bmatrix} = 0. \tag{29}$$

The determinant of the square matrix has to vanish for nontrivial solutions to exist. This is easily shown to be the same as the determinant in Eq. (6) and yields the same equation for β, Eq. (7). The structure of the solution at $x \geqslant a$ is therefore much the same as given by the linear theory, consisting of three additive contributions to each of ζ_i ($i = 1, 2, 3$), corresponding to the three roots β_j ($j = 1, 2, 3$). The boundary conditions at infinity are the same, $\zeta_i \to 0$, but they differ at $x = a$, the shoreward bound of the three-layer system. Here the conditions are that the top-layer thickness vanishes and that the second interfaces and the bottom two layer velocities join smoothly:

$$\left.\begin{aligned} \zeta_2 &= \zeta_1 + h_1 \\ \zeta_{3-} &= \zeta_{3-}, \qquad (x = a) \\ \left.\frac{d\zeta_3}{dx}\right|_- &= \left.\frac{d\zeta_3}{dx}\right|_+ \end{aligned}\right\}, \tag{30}$$

where subscripts $-$ and $+$ designate values infinitesimally to the left and right of $x = a$, respectively.

It is thus necessary to consider also the two-layer adjustment problem at $x \leqslant a$. Here geostrophic balance and potential vorticity conservation are expressed by

$$\left.\begin{aligned} -fv_2 &= -g\frac{d\zeta_2}{dx} \\ -fv_3 &= -g\frac{\rho_2}{\rho_3}\frac{d\zeta_2}{dx} - g\epsilon_{23}\frac{d\zeta_3}{dx} \\ \frac{dv_2}{dx} &= f\frac{\zeta_2}{h_2} - f\frac{\zeta_3}{h_2} \\ \frac{dv_3}{dx} &= f\frac{\zeta_3}{h_3} \end{aligned}\right\}. \tag{31}$$

Again using the notation of Eq. (28), but with $\beta = \beta_*$ on elimination of v_2, v_3, the following equations for the interfaces emerge:

$$\begin{bmatrix} 1 - \dfrac{\beta_*}{h_2} & \dfrac{\beta_*}{h_2} \\ \dfrac{\rho_2}{\rho_3} & \epsilon_{13} - \dfrac{\beta_*}{h_3} \end{bmatrix} \times \begin{bmatrix} \zeta_2 \\ \zeta_3 \end{bmatrix} = 0. \tag{32}$$

Note that at $x \leqslant a$ the top of the second layer coincides with the free surface, i.e., $\zeta_2 = h_1 + O(\delta H)$, where δ is a small quantity. The boundary condition at the coast is zero cross-shore displacement in the course of the adjustment process. The longshore momentum equations are, in the absence of longshore pressure gradients and internal friction:

$$\left.\begin{aligned} \frac{dv_1}{dt} &= -fu_1 + \frac{F}{h_1} \\ \frac{dv_2}{dt} &= -fu_2 \\ \frac{dv_3}{dt} &= -fu_3 \end{aligned}\right\}, \tag{33}$$

where the time derivatives are total. At the coast, $u_i = 0$ and, if layers 2 and 3 remain attached to the coast:

$$v_2 = v_3 = 0, \quad (x = 0) \tag{34}$$

The velocities at $x > 0$ are, by Eqs. (31), proportional to the degree of stretching experienced by the two layers. A special case, which will turn out to be of interest, is when the two bottom layers are equally stretched, i.e.,

$$\frac{\zeta_2 + h_2 - \zeta_3}{h_2} = \frac{\zeta_3 + h_3}{h_3}, \tag{35}$$

or, solving for the ratio ζ_3/ζ_2

$$\frac{\zeta_3}{\zeta_2} = \frac{h_3}{h_2 + h_3}. \tag{35a}$$

Eqs. (32) are consistent only if the determinant of the square matrix vanishes, i.e., if

$$\beta_*^2 - \beta_*(h_2 + h_3) + \epsilon_{23}h_2h_3 = 0. \tag{36}$$

The two roots are, to the lowest order in ϵ_{23},

$$\left.\begin{aligned}\beta_{*1} &= h_2 + h_3 + O(\epsilon H)\\ \beta_{*2} &= \frac{\epsilon_{23}h_2h_3}{h_2+h_3} + O(\epsilon^2 H)\end{aligned}\right\}. \tag{37}$$

In addition to determining β_*, Eqs. (32) also yield the relationship of the displacements ζ_2 and ζ_3 for fixed β_*:

$$\zeta_3 = \zeta_2\left(1 - \frac{h_2}{\beta_*}\right). \tag{38}$$

Thus, in the barotropic mode, $\beta_* = \beta_{*1} \approx h_2 + h_3$,

$$\frac{\zeta_3}{\zeta_2} = \frac{h_3}{h_2+h_3}, \tag{39}$$

a result identical with Eq. (35a). In this mode, given that $\zeta_2 = h_1 + O(\delta H)$, the lower interface shape is thus nearly horizontal, $\zeta_3 \approx h_1h_3/(h_2+h_3) + O(\delta H)$. Where the barotropic mode only is excited, the second interface rises to this nearly constant new depth.

The internal mode, $\beta_* = \beta_{*2}$, is characterized by very different interface displacements, ζ_3 = order $\times (\epsilon^{-1}\zeta_2)$, but its influence is restricted to horizontal boundary layers of scale width $R_2^* = \sqrt{g\beta_{*2}}$. Thus if $a \gg R_2^*$, any internal mode excitation present near $x = a$ decays to a negligible amplitude at the coast. Because the boundary conditions at the coast can be satisfied without internal readjustment [as in a two-layer system shoreward of the outcropping of the single interface [Csanady (1977)] no interface distortion occurs here, the interface between the second and third layers remaining flat (to order δ). As in the linear theory, $d\zeta_3/dx$ must vanish at the coast in view of the boundary condition (34). Its shape may in fact easily be seen to be proportional to $\delta H \cosh(x/R_1^*)$, with $R_1^* = (g\beta)_{*1}^{1/2}$, if $a \gg R_2^*$. Thus, the second interface rises no higher than $\zeta_3 = h_1h_3/(h_2 + h_3) + O(\delta H)$, the level determined by the principle of equal stretching. This verifies the hypothesis made at the beginning of the present section, that the bottom interface remains submerged.

In the neighborhood of the top interface outcropping, $x = a$, the interface shapes may be written, neglecting barotropic mode contributions of order δ and of order ϵ, and supposing $a \gg R_2^*$:

$$\left.\begin{aligned}\zeta_3 &= \frac{h_1h_3}{h_2+h_3} - A\exp[(x-a/R_2^*], \quad (x \leqslant a)\\ \zeta_2 &= B\exp[-(x-a)/R_2]\\ &\quad + C\exp[-(x-a)/R_3], \quad (x \geqslant a)\\ \zeta_3 &= (1-\mu_2)B\exp[-(x-a)/R_2]\\ &\quad + (1-\mu_3)C\exp[-(x-a)/R_3]\end{aligned}\right\}, \tag{40}$$

with $\mu_i = \epsilon_{12}h_2/\beta_i$, $i = 2, 3$.

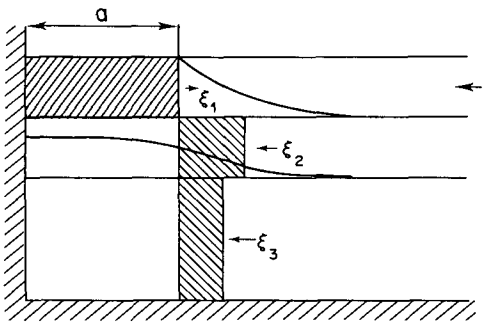

FIG. 9. Mass balance of displaced layers at $x = a$: oppositely shaded areas are equal, top layer outflow being balanced by inflow in the bottom two layers, with greater shoreward displacement in intermediate layer.

Applying the conditions expressed in Eqs. (30), with the neglect of $\zeta_1 = O(\delta + \epsilon)$, it is possible to determine the three constants A, B and C. This fully determines (to zeroth order in ϵ and δ) the interface shapes near the pycnocline outcropping for the asymptotic case of a large enough wind impulse to produce $a \gg R_2^*$.

To calculate the magnitude of a for a given wind impulse $I = Ft$ it may be supposed that $a \ll R_1$ (the radius of deformation in the barotropic mode), in which case the fluid column displacements across $x = a$ balance to zeroth order (Fig. 9):

$$\xi_i h_i = 0 \quad \text{(sum)}, \tag{41}$$

where $\xi_i = \int u_i' dt$, $u_i'(t)$ being the cross-shore velocity at time t of the fluid column ending up at $x = a$ after adjustment.

The time-integrated form of Eqs. (33) now yields, noting that $\xi_1 = a$ for the top layer fluid at $x = a$ after adjustment,

$$ah_1 = \frac{v_2h_2}{f} + \frac{v_3h_3}{f}. \tag{42}$$

The first of (33) on time integration also yields

$$v_1 = \frac{I}{h_1} - fa. \tag{43}$$

The velocities v_2 and v_3 may be expressed from Eqs. (27) as v_1 plus terms proportional to interface slopes. Substituting into (42) and eliminating v_1 with the aid of (43), gives, to the lowest order in ϵ

$$a = \frac{I(h_2+h_3)}{fh_1H} + \frac{1}{f^2H} \times \left\{\epsilon_{12}g(h_2+h_3)\frac{d\zeta_2}{dx} + \epsilon_{23}gh_3\frac{d\zeta_3}{dx}\right\}. \tag{44}$$

The bracketed term is negative and its precise value varies weakly with a, becoming constant for

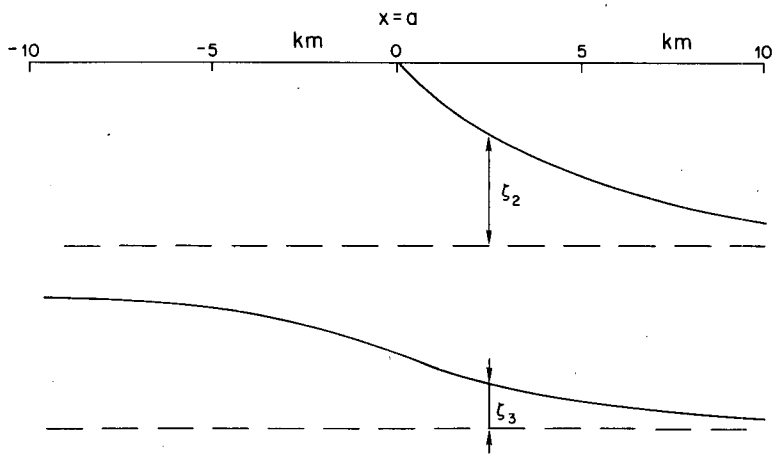

FIG. 10. Calculated interface shapes near the surface outcropping of the top interface, for large offshore displacement a.

$a \gg R_2^*$, as may be seen from the discussion above. Thus, as in the two-layer case (Csanady, 1977), some minimum impulse is necessary to bring the top interface to the surface. Once a becomes large enough, its further dependence on I is linear, again as in the two-layer case. In this asymptotic stage the second term on the right of Eq. (44) effectively replaces the (negative) internal radius of deformation of the two-layer model.

If the same numerical example is taken as before, one calculates $R_2^* = 3.35$ km for the internal radius of deformation at $x \leq a$, after the top interface moved sufficiently far offshore. The calculations of the constants in Eq. (40) yield

$$\frac{A}{h_1} = 0.35, \quad \frac{B}{h_1} = 1, \quad \frac{C}{h_1} = 0, \tag{45}$$

to within $\epsilon^{1/2}$. The second term on the right of (44) is 3.9 km, so that $a = 10$ km is generated by an impulse of $I = 26$ m^2 s^{-1}. This is high for a single impulse (20 m s^{-1} wind acting for 8 h) but certainly not unrealistic. Fig. 10 illustrates calculated conditions near $x = a$.

Cross-shore water column displacement in the surface layer just under the frontal outcropping are in this case $a = 10$ km. If the bottom layers moved together, they would compensate with an offshore displacement of 2.5 km. In the three-layer example, however,

$$-\xi_2 = 2.5 + (A/h_2)R_2^* = 3.67 \text{ km},$$

$$-\xi_3 = 2.5 - (A/h_3)R_2^* = 2.11 \text{ km}.$$

Thus there is considerable relative motion between the layers, mainly between layers 1 and 2 ($\Delta\xi = 13.67$ km) but also between layers 2 and 3 ($\Delta\xi = 1.56$ km). One should remember further that only the quasigeostrophic response has been calculated here: near-inertial oscillations excited in addition involve almost-periodic displacements of the same order.

6. Discussion

What can one usefully learn from highly idealized models such as discussed above? Constant total depth, neglect of mixing and internal friction, and impulsively exerted wind stress are certainly gross overidealizations. Nevertheless, the calculations reveal some key characteristics of the inertial response of a stratified fluid to forcing directly applied to the top layer alone. Compared to the two-layer model discussed in detail earlier, the extra information concerns what happens when the density differences between layers below the surface mixed layer are about as large as the density jump at the base of the mixed layer.

One important general recognition is that the wind "peels off" the surface layer over which it acts, bringing only the next lighter layer to the surface, without causing the second (or third, or fourth) interface to move upward by more than a fraction of its initial depth. In the absence of a direct external force acting on the lower layers, their longshore acceleration is due solely to cross-shore adjustment drift. At a vertical coast, where all cross-shore velocities vanish, no longshore velocities arise and density interfaces remain horizontal. Significant interface tilts develop only in internal boundary layers of scale width R_2: this follows from the structure of the governing equations on the principle discussed by Carrier (1953). Because at the shore the lower interface(s) remains (remain) horizontal, no internal boundary layer is required there.

In a qualitative way this result should remain valid over a sloping bottom, as may be seen by reference

to Fig. 11. Consider the case again when the top interface–surface intersection is far offshore and the water from lower layers has replaced top-layer fluid nearshore. Little reflection shows that the boundary conditions at the coast may be satisfied if *all* fluid columns (in both lower layers) are displaced shoreward by the same distance b, generating constant velocity $v_2 = v_3 = fb$ toward positive y. The second interface then remains horizontal, except again in the neighborhood of the surface outcropping of the top interface.

It also follows quite generally that internal mode adjustments of interface shape remain confined to within distances of order R_2 of the top interface outcropping. A coastal jet appears within this range, but beyond that the response is the same as in a homogeneous fluid. This result is the same as one finds from a two-layer model, except that it is now seen to apply to the bottom interface as well (and, by reasonable inference, other interfaces, for multilayer models).

A further general result, peculiar to a model with at least three layers, is the recognition of considerable relative motion between the lower layers. On account of the different shape of the top and bottom interfaces near the top interface outcropping, itself a direct consequence of longshore velocity differences or their absence, the second layer becomes thicker (the isopycnals "open up" somewhat) on the shore side and thinner further offshore for compensation, than the equally-stretched limit far from the outcropping. The associated cross-shore relative displacements are of a large amplitude, of the order of kilometers.

Another result, not so far discussed explicitly, is that an opposite wind impulse, which causes downwelling, again affects the top interface more than the bottom one, close to shore. In such an event the top interface is depressed more than the bottom one, squeezing the intermediate-density fluid away from the coast. The cross-shore displacements predicted by theory for upwelling or downwelling are of the same order. Hence, an alternation of upwelling and downwelling events acts as a sort of "bellows" mechanism, moving intermediate density fluid in and out of the coastal band. Since in the real case such inertial effects are likely to be accompanied by considerable vertical mixing, the bellows mechanism is likely to be an important instrument of cross-shore mass exchange.

It remains to note here previous models of transient upwelling due to Allen (1973) and Pedlosky (1974, 1978). These are based on boundary layer theory, but the equations governing the interior flow are effectively the same as Eqs. (1), or their nonlinear analogs, except for the assumption of continuous stratification rather than discrete layers. This is not an important difference in itself, at least for the linear theory, because the response of the stratified interior can be reduced to a sum of normal modes, much as the three layer system discussed earlier. The major difference lies in the hypothesis made by both Allen and Pedlosky that the interior flow is forced entirely by a continuous sink at the surface–coast corner, where a surface Ekman layer originates, driven by a sustained wind. This idealization involves the hypothesis that the fluid continually drawn into the "sink" is able to move offshore in the surface Ekman layer. Since in a stratified fluid surface density is less than the density of the lower layers supplying the sink, this requires appropriate surface heating or freshening, so that the model is diabatic. By contrast, the previous calculations were made supposing that fluid columns conserve their density. On this hypothesis, Ekman transport advects surface layer fluid offshore ultimately to the point where the top interface comes to intersect the free surface. From the observational evidence it would appear that an adiabatic model constitutes a more realistic idealization of rapidly developing transient upwelling than a diabatic model requiring a fairly large heat or freshwater input at the coast. One should add, however, that mixing of overlying layers by a strong wind is not negligible, generating some intermediate density fluid that may well escape along a mid-level isopycnal surface. This, and other similar questions, are clearly outside the scope of the present investigation.

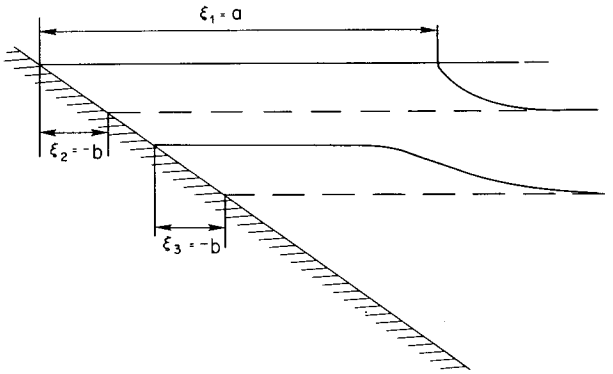

FIG. 11. Three-layer fluid over inclined plane beach, after development of full upwelling. Shoreward displacements of fluid columns near the coast are equal in both lower layers, and so therefore are longshore velocities. The second density interface consequently remains horizontal, except in the region of the top interface outcropping.

Acknowledgments. The work described herein was supported by a contract entitled "Coastal Shelf Transport and Diffusion" from the Department of Energy and, prior to December 1980, also by the Great Lakes Environmental Research Laboratory of NOAA at Ann Arbor. It forms the substance of a lecture given at a session of the American Society

of Limnology and Oceanography in honor of C. H. Mortimer. I would like to record my indebtedness to Dr. Mortimer for much inspiration and encouragement during my first attempts to approach the dynamical problems of the Great Lakes.

REFERENCES

Allen, J. S., 1973: Upwelling and coastal jets in a continuously stratified ocean. *J. Phys. Oceanogr.*, **3,** 245–257.

Carrier, G. F., 1953: Boundary layer problems in applied mechanics. *Adv. Appl. Mech.*, **3,** 1–19.

Charney, J. G., 1955: Generation of oceanic currents by wind. *J. Mar. Res.*, **14,** 477–498.

Crépon, M., 1967: Hydrodynamique marine en regime impulsionnel. *Cah. Oceanogr.*, **19,** 847–880.

Csanady, G. T., 1973: Wind-induced barotropic motions in long lakes. *J. Phys. Oceanogr.*, **3,** 429–438.

——, 1977: Intermittent 'full' upwelling in Lake Ontario. *J. Geophys. Res.*, **82,** 397–419.

Halpern, D., 1976: Structure of a coastal upwelling event observed off Oregon during July 1973. *Deep-Sea Res.*, **23,** 495–508.

Huyer, A., E. J. Sobey and R. L. Smith, 1979: The spring transition in currents over the Oregon continental shelf. *J. Geophys. Res.*, **84,** 6995–7011.

Mortimer, C. H., 1952: Water movements in lakes during summer stratification: evidence from the distribution of temperature in Windermere. *Phil. Trans. Roy. Soc. London*, **B236,** 355–404.

——, 1963: Frontiers in physical limnology with particular reference to long waves in rotating basins. Pub. No. 10, Great Lakes Res. Div., University of Michigan, 9–42.

Pedlosky, J., 1974: Longshore currents and the onset of upwelling over bottom slope. *J. Phys. Oceanogr.*, **4,** 310–320.

——, 1978: A nonlinear model of the onset of upwelling. *J. Phys. Oceanogr.*, **8,** 178–187.